Structural and electronic properties of tin clathrate materials

Charles W. Myles
Department of Physics, Texas Tech University, Lubbock, Texas 79409-1051

Jianjun Dong
Physics Department, Auburn University, Auburn, Alabama 36849-5311

Otto F. Sankey
Department of Physics and Astronomy and Materials Research Center, Arizona State University, Tempe, Arizona 85287
(Received 12 April 2001; published 2 October 2001)

Using an *ab initio* local density approximation (LDA) method, we have studied the structural properties and the electronic band structures of several tin-based clathrate materials. We find that the pure type-I (Sn_{46}) and type-II (Sn_{136}) clathrate frameworks are metastable, expanded-volume phases of Sn and that they are *semiconductors*. We further find that the Cs encapsulated type-I binary clathrate is metallic if full stoichiometry (Cs_8Sn_{46}) is assumed. However, our calculations suggest that vacancy formation is energetically favored, and that the stable vacancy compound $Cs_8Sn_{44}\square_2$ is a narrow gap semiconductor. We have also studied the ternary clathrate compounds $Cs_8Ga_8Sn_{38}$ and $Cs_8Zn_4Sn_{42}$, which have been suggested as potential thermoelectrics, and we find that these are semiconductors. The trends in the structural and electronic properties of these Sn-based clathrates are discussed, and our results are compared with experiment where possible.

DOI: 10.1103/PhysRevB.64.165202 PACS number(s): 71.20.Nr, 71.20.Mq, 61.66.−f

I. INTRODUCTION

The two common solid phases of elemental tin (Sn) are gray tin and white tin. Gray tin, also known as α-Sn, has two atoms per primitive face-centered cubic (fcc) cell in the diamond crystal structure. White-tin, also known as β-Sn, has two atoms per primitive body-centered tetragonal (bct) cell. Another solid phase of Sn is the high-pressure γ-Sn phase, which also has a bct crystal structure, but with four atoms per primitive cell.[1] Similar to the lighter group-IV (B) elements C, Si and Ge, Sn atoms can form sp^3 tetrahedral bonds and the diamond structure α-Sn is the stable ground state phase at low temperatures. In contrast to the diamond structure phases of C, Si, and Ge, which are well known semiconductors α-Sn is a semimetal. Tin is also able to form octahedral bonds. Both β-Sn and γ-Sn are octahedrally bonded, and they are metals. It is interesting to note that the minimum binding energy of the β-Sn phase is energetically very close to that of the ground state, α-Sn phase, despite the significant difference in the bonding in the two phases. The entropy driven $\alpha \rightarrow \beta$ phase transition proceeds at a temperature of 13 °C at ambient pressure.[2]

Tin atoms, as well as atoms of Si and Ge, can also form novel open-framework cagelike solids called clathrates. In these structures, all internal cages are strongly bonded, with all atoms in fourfold connected, sp^3-like configurations. The clathrate frameworks were first discovered in the hydrate (ice) materials.[3] Starting in the mid 1960's, it was found that Si and Ge can form clathrate frameworks with guest metal atoms (Na or K) encapsulated into the ''cages'' of the structure.[4–9] Since then, a wide variety of Si and Ge clathrates have been synthesized and characterized and the understanding of these novel materials is advancing rapidly. Silicon clathrates have been the most theoretically studied of this material class. An early theoretical study of the Si clathrates was performed by Adams *et al.*,[10] who used a local-orbital tight-binding-like LDA method. That study focused on the pure Si clathrates. Other calculations have been performed on Si clathrates by several groups.[11–15] Recently, calculations have also been performed on Ge clathrates by two of us[16,17] and by others.[18] The Sn clathrates have received less attention than their Si and Ge counterparts and only recently have been synthesized.[19–21] Here, we report *ab initio*, density functional planewave pseudopotential calculations of the structural and electronic properties of several Sn-based clathrate materials.

The first motivation for the present work is to obtain a systematic understanding of the intrinsic properties of the (as yet unsynthesized) clathrate phases of pure (guest-free) elemental Sn, and their relation to the ''compact'' α-Sn phase. A theoretical study of the pristine Sn clathrates is the first step in understanding the more complex laboratory-synthesized Sn clathrate compounds. Our calculations show that the energy cost to form clathrate phases compared to the α phase is small for Sn; less than the analogous energy increase in the Si clathrates but similar to that in the Ge clathrates. In addition, we find that the ''band-gap opening'' effect previously found in the Si and Ge clathrates is also present in the Sn clathrates; our results show that both the type-I (Sn_{46}) and type-II (Sn_{136}) clathrate phases are semiconductors. This has the important and interesting consequence that, if they could be synthesized, the pure Sn clathrates would be the first semiconducting materials made from elemental Sn.

Most laboratory-synthesized group-IV (B) clathrates, including those based on Sn, are not elemental crystals, but are compounds in which alkali atoms are incorporated inside the cages as guests. Because of the open framework in the clathrates, many possible guest atoms can be present in the cages, and these can substantially alter the material properties. Varying the guest species and concentration can give a ma-

terial designer a means by which to ''tune'' the material properties. A second motivation of the present study is to obtain an understanding of the effects of such guest atoms on the ''tuning'' of the structural and electronic properties of the Sn-based clathrates. As a first step in obtaining an understanding of the effects of guests in the Sn-based clathrates, here we concentrate only on the type-I framework and consider only Cs guests. The sizes of the cages in the Sn clathrates are the largest of the group-IV (B) clathrates, providing the possibility of a wide variety of guest species. In addition, the Sn-Sn bond is relatively weak (compared with Si-Si or Ge-Ge bonds) and this may influence the guest-host interactions. The first three reports of the synthesis of alkali-doped Sn clathrates[19–21] found this to be true; extensive Sn vacancies were found in the framework.

The earliest work on alkali-doped group-IV (B) clathrates assumed full stoichiometry and interpreted x-ray diffraction experiments on this basis. See for example, the early reports on Na_8Si_{46},[4] K_8Ge_{46},[6,7] and Cs_8Sn_{46}.[22] However, based on a careful interpretation of x-ray data, Zhao and Corbett proposed that two vacancies (per unit cell) are formed in the Rb-Sn and K-Cs-Sn type-I clathrate compounds, and that the correct compositions should be $Rb_8Sn_{44.6}\square_2$ and $K_{1.6}Cs_{6.4}Sn_{44}\square_2$ (Ref. 19) (where $\square$ indicates a vacancy on a framework site). This raises the interesting and important issue of vacancy formation and the energetics of such a process in the group-IV (B) clathrate compounds. It should be pointed out that this phenomenon is intrinsically related to the open cagelike frameworks of the clathrates and to the doping effects of the guests, in which the effective ''doping concentration'' can be at least three orders of magnitude higher than that in the most heavily doped diamond structure Si.[23]

Although vacancy formation can be qualitatively interpreted as caused by a weakening of the framework bonds due to electron transfer from the guest atoms to the framework antibonding levels (conduction bands), the detailed physics of this phenomenon is more complex. Furthermore, vacancy formation and its energetics depends significantly on which group-IV element forms the clathrate framework. A quantitative reexamination the type-I Na-Si clathrate compounds by solid state ^{29}Si NMR and x-ray refinement has revealed no detectable Si vacancies, so that the composition is Na_8Si_{46}.[24] The full stoichiometry of the framework sites was also confirmed in $K_{8-\delta}Si_{46}$ and $Rb_{6+\gamma}Si_{46}$.[25] Vacancy formation remains controversial in the Ge clathrates. Ramachandran *et al.* have found two Ge vacancies per unit cell (at 6*c* sites) in $K_{8-\delta}Ge_{44}\square_2$ and $Rb_{6+\gamma}Ge_{44}\square_2$,[25] similar to what is found in the Sn clathrates. However, no vacancies have been found by Bobev and Sevov in their $Na_8Cs_{16}Ge_{136}$ samples.[26] Understanding the energetics of vacancy formation in the Cs-Sn clathrate compounds and the role that vacancies play in ''tuning'' the properties of these materials are two of the motivations for this study.

A final motivation for this work is to study the basic properties of an interesting class of alloyed Sn clathrate compounds which have recently been shown to have potential thermoelectric applications. A good thermoelectric must have a high Seebeck coefficient, a high electrical conductivity, and a low thermal conductivity.[27–29] Because of correlations among these properties, it is difficult to simultaneously optimize all of these conditions. A new and interesting direction in the search for desirable thermoelectric systems is to explore the properties of guest-containing open-framework materials. Introducing specific guests into the host frameworks usually produces low frequency, ''rattling'' vibrational modes. These can strongly scatter the heat-carrying acoustic modes.[30] This concept has been successful in the skutterudites.[32–34]

Guided by these notions, Nolas *et al.*[35,36] have shown that Ge-based clathrates with Sr guests in the cages ($Sr_8Ga_{16}Ge_{30}$) have a remarkably low thermal conductivity. Recent atomistic simulations of the heat current[37] have shown that amorphous Ge and the type I Ge clathrate frameworks containing guest ''rattlers'' have comparable thermal conductivities, as was suggested by Slack[29,30] and as has been seen experimentally.[35,36,31] Recently, low thermal conductivities in some Sn-based clathrate alloys, such as $Cs_8Ga_8Sn_{38}$ and $Cs_8Zn_4Sn_{42}$ have also been reported by Nolas *et al.*[21] These two experimentally relevant ternary alloyed Sn clathrates are examined in the present study.

There have been several recent experimental studies of Sn-based clathrates. However, to our knowledge, no theoretical study of these materials has yet been reported. The properties of interest in the present work are the equations of state, the crystalline structural parameters, the energetics of spontaneous vacancy formation, and the electronic band structures. Calculations of the vibrational spectra, which are important for material characterization and are also a key to understanding the material thermal conductivity, will be reported elsewhere.[38]

Six Sn-based clathrate material systems have been chosen for our study. These can be classified into three categories. These are (1) the two elemental framework clathrates Sn_{46} (type I) and Sn_{136} (type II), (2) two binary compounds based on type-I Sn clathrates with Cs guests: the fully stoichiometric compound Cs_8Sn_{46} and the vacancy compound $Cs_8Sn_{44}\square_2$, and (3) two ternary compounds based on type-I Sn clathrates with Cs guests and with groups III or II substitutional atoms alloyed at framework sites: $Cs_8Ga_8Sn_{38}$ and $Cs_8Zn_4Sn_{42}$.

II. COMPUTATIONAL APPROACH; α-TIN AND β-TIN RESULTS

Our calculations are based on an *ab initio* density functional planewave method.[39,40] The local density approximation (LDA) to density functional theory is used to describe electron correlation effects and the electron exchange-correlation energy is approximated with the Ceperley-Alder functional.[41] This method has been extensively tested on a wide variety of systems. The implementation we use is particularly efficient for the large clathrate unit cells. This technique has been adopted in our previous studies of Si (Refs. 14,24) and Ge (Refs. 16,17) clathrates. In those studies, the calculated structural and vibrational properties were found to be in good agreement with experiment.[7,9,35,42] The effects of the generalized gradient approximation (GGA) correction to

TABLE I. LDA-calculated lattice parameters a and c, relative binding energies E_0, and bulk moduli K_0 of α-Sn and β-Sn compared with experimental data and with previous LDA calculations. The minimum binding energies of β-Sn are shown in parentheses, with respect to that of α-Sn .

		Present Study	Previous LDA Calculations	Experiment
α-Sn	a (Å)	6.46[a], 6.48[b]	6.40[c], 6.55[d], 6.38[e]	6.48[f]
	E_0 (eV/atom)	−4.484[a], −4.485[b]		
	K_0 (GPa)	44.3[a], 44.9[b]	51.2[c], 44.7[d], 47.0[e]	53.0[f]
β-Sn	a (Å)	5.78[a], 5.79[b]	5.70[c], 5.70[e]	5.82[f]
	c/a ratio	0.541[a], 0.541[b]	0.545[c], 0.541[d], 0.544[e]	0.546[f]
	E_0 (eV/atom)	(−0.017)[a], (−0.026)[b]	(+0.034)[c], (+0.010)[d], (+0.022)[e]	
	K_0 (GPa)	58.9[a], 60.0[b]	60.5[c], 54.4[d], 61.0[e]	55.0[f]

[a]Without the $4d$ semicore electrons included.
[b]With the $4d$ semicore electrons included.
[c]Reference 45.
[d]Reference 46.
[e]Reference 47.
[f]References 45 and 47.

the LDA were examined in Ref. 14 and were found to be minor. Thus, we neglect these corrections here.

In this study, we use ultrasoft pseudopotentials[43,44] to approximate the effects of the core and semicore electrons. Although semicore electron effects are known to be more important in Sn than in Si and Ge, in our calculations of the properties of the Sn-based clathrates, our computational resources have limited us to an explicit treatment of only the Sn valence ($5s^2 5p^2$) electrons. The clathrate unit cells are large and complex ($\sim$50 atoms). Thus, adding the semi-core ($4d^{10}$) electrons to the calculations would significantly increase their already significant computational intensity. We have tested this approximation on α-Sn and β-Sn, which have much smaller unit cells than the clathrates. The results of this test are summarized in Table I. In that table, we show our LDA-calculated lattice parameters, relative binding energies, and bulk moduli for α-Sn and β-Sn. Also shown for comparison are the results of previous LDA calculations[45–47] and relevant experimental data. We have used $10\times10\times10$ and $8\times8\times8$ Monkhorst-Pack k-point grids in our α-Sn and β-Sn calculations, respectively. The planewave cutoff was 12.9 Ryd. Since Sn is much heavier than C, Si, and Ge, relativistic effects can be important in determining its properties. Our calculations use a scalar relativistic approximation which neglects spin-orbit coupling. Spin-orbit coupling can split degenerate electronic states, but it has a relatively small effect on binding energies. We note that the previous LDA results[45–47] which are listed in Table I also have neglected spin-orbit coupling.

As is shown in Table I, if the $4d$ semi-core electrons of Sn are included in our calculations, we find that the β-tin phase is the ground state by the small energy 17 meV/atom in comparison with the α-Sn phase. If these semi-core electrons are neglected, this energy increases to 26 meV/atom. It is well known[47] that the order of the energetics is reversed in nonrelativistic LDA calculations and that α-Sn has a slightly lower energy at zero temperature. Our failure to obtain the correct relative energetics for the two most common elemental Sn solids may be due to the fact that we have neglected spin-orbit coupling. We have repeated the calculations in the GGA, and the results are similar to the LDA results. We feel that this minor error in the energetics of the α-Sn and β-Sn phases should have little effect on our predicted properties of the Sn-based clathrate phases, which are the focus of this paper. We believe that this error is most prominent when the minimum binding energies for β-Sn and α-Sn are compared, because the bonding in these two structures is very different. A comparison of our calculated minimum binding energies of α-Sn and the Sn clathrate structures should be more reliable, since the bonding in these systems is similar.

For the clathrate systems, the total energy calculations have been performed over a $4\times4\times4$ Monkhorst-Pack k-point grid. Group theory has been used to reduce the computational effort required to determine the energies and forces during structural optimization. To determine the optimized structure for each material, we have first chosen a fixed unit cell volume, and we have then optimized the ionic positions by minimizing the total (binding) energy through a conjugate gradient algorithm using atomic forces. This process has been repeated for several unit cell volumes, from which an equation of state and a global minimum energy can be determined. Finally, the internal coordinates are optimized at the minimum energy volume. Since the type-I and type-II clathrate structures are cubic (see Sec. III B), optimizing the external lattice (in this case, a single lattice constant a) is straightforward. The equilibrium structural parameters, the electronic band structures, and the vibrational modes[38] have been evaluated at the minimum energy configuration.

For each material, the LDA energy vs volume curve which results from the procedure just described has been fit with the Birch-Murnaghan equation of state (EOS).[48,49] This fitting determines the minimum binding energy E_0 (the binding energy compared to that of the free atoms), the corresponding volume V_0, the equilibrium bulk modulus K_0, and its pressure derivative $K' = dK_0/dP$.

III. ELEMENTAL TIN CLATHRATE MATERIALS

A. Equations of state and energetics

The Birch-Murnaghan parameters resulting from the fits for the pure Sn clathrate framework materials Sn_{46} and

TABLE II. The parameters of the Birch-Murnaghan equation of state for α-Sn and for the elemental Sn clathrates obtained from a fit to the LDA energy vs volume curve.

Phase	E_0 (eV/atom)	V_0 (Å^3/atom)	K_0 (GPa)	K'
α-Sn	−4.484	33.75	44.3	4.8
Sn_{46}	−4.443	37.91	38.4	4.9
Sn_{136}	−4.446	38.34	38.5	5.0

Sn_{136}, along with those for α-Sn, are listed in Table II. Plots of the fitted EOS curves (at $T=0$ K) for the pure Sn clathrates along with those for α-Sn and β-Sn, are shown in Fig. 1. As can be seen from the figure, the type-I and type-II Sn clathrates are both *expanded* phases of elemental Sn and their EOS's are very close to each other in energy at all volumes. Compared with α-Sn, their unit cell volumes are expanded by the rather large amount of 12–14 %. Further, the predicted minimum binding energies for the clathrates, shown in Table II, are only 38–41 meV/atom higher than that for the α-Sn phase. Since 40 meV is only about 464 K in temperature units, the minimum energy difference between the Sn clathrate frameworks and the α-Sn phase is very small; of the order of k_BT at room temperature. This indicates that these clathrate phases are energetically metastable. [The corresponding energy difference between the diamond and clathrate phases for Si was found to be about 70 meV/atom,[14] while this difference for Ge (Ref. 16) was found to be about 50 meV/atom.] It is also significant that such a small energy increase is accompanied by the relatively large volume increase already mentioned. The bulk moduli of the two types of Sn clathrate frameworks are similar to each other, and are about 13% smaller than that of the α-Sn structure.

B. Structures and internal coordinates

The local bonding in the group-IV clathrates is similar to that in the diamond structure. However, in the clathrates, pentagonal rings of atoms are present, making the topology quite different from that of the diamond structure. There are two clathrate frameworks, simple cubic (sc) type-I, for which the space group is $Pm\bar{3}n$, No. 223, and face centered cubic (fcc) type-II, for which the space group is $Fd\bar{3}m$, No. 227. More detailed discussions concerning the general structural and geometric properties of the clathrates may be found in our previous studies of silicon[10,11,14] and germanium[16] clathrates and in the references in those papers.

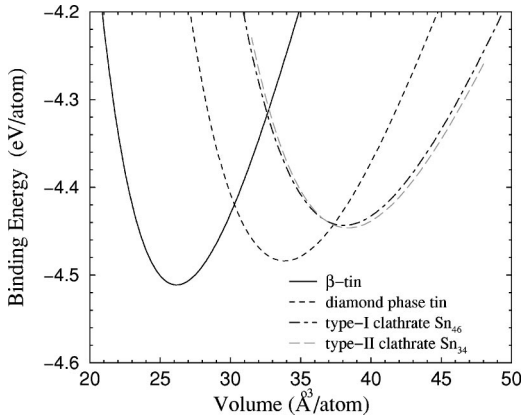

FIG. 1. Equations of state (energy vs volume) of four Sn phases: α-Sn (diamond), β-Sn, Sn_{46}, and Sn_{136}. The LDA-calculated data has been fit to the Birch-Murnaghan equation. Table I gives the resulting parameters.

TABLE III. Theoretical structural parameters for Sn-based clathrate materials at the volume of the minimum energy. The LDA-optimized lattice constant is a. (Experimental results for related materials are summarized in Table V for comparison.) For Sn_{136}, the symmetry sites are $8a$ $(\frac{1}{8},\frac{1}{8},\frac{1}{8})$, $32e$ (x_e,x_e,x_e), and $96g$ (x_g,x_g,z_g). For the type-I frameworks based on Sn_{46}, the symmetry sites are $6c$ $(\frac{1}{4},0,\frac{1}{2})$, $16i$ (x_i,x_i,x_i), and $24k$ $(0,y_k,z_k)$. The internal coordinates of $Cs_8Sn_{44}\square_2$, $Cs_8Ga_8Sn_{38}$, and $Cs_8Zn_4Sn_{42}$ are not listed because these materials do not have the same symmetry as Sn_{46} and Cs_8Sn_{46}.

Material	a (Å)	Fractional internal coordinates
Sn_{136} (type-II)	17.34	$x_e=0.2171$, $x_g=0.1824$, $z_g=0.3704$
Sn_{46} (type-I)	12.04	$x_i=0.1833$, $y_k=0.3084$, $z_k=0.1167$
Cs_8Sn_{46}	12.37	$x_i=0.1843$, $y_k=0.3074$, $z_k=0.1184$
$Cs_8Sn_{44}\square_2$	12.03	
$Cs_8Ga_8Sn_{38}$	11.95	
$Cs_8Zn_4Sn_{42}$	12.03	

The two pure Sn clathrates (Sn_{46} and Sn_{136}), are expanded volume phases of elemental Sn. At present, both of these structures remain hypothetical; all Sn-based clathrates which have been synthesized contain guest atoms. Our optimized structural parameters (cubic lattice constant and relative internal coordinates) for Sn_{46} and Sn_{136} are shown in Table III. The Sn-Sn bond-angles we obtain deviate from the ideal tetrahedral angle of 109.5°, ranging from 104.3°–124.8° in Sn_{46}, and from 105.6°–119.8° in Sn_{136}. The bond angle spread in the Sn clathrates is similar to the results found in our previous studies of Si and Ge clathrates. We find four distinct Sn-Sn bond lengths in each clathrate type. For Sn_{46}, these are 2.77, 2.78, 2.80, and 2.81 Å, and for Sn_{136} these are 2.77, 2.796, 2.797, and 2.82 Å. These should be compared with our optimized tetrahedral Sn-Sn bond length in α-Sn of 2.80 Å. Comparing the type I and type II Sn clathrates, we find that Sn_{46} has a slightly larger bond angle spread (20.5° vs 14.2°) than Sn_{136}. However, the bond length and bond angle spreads in both clathrate types are small enough to indicate that the formation of these structures should not be energetically very costly, which is in agreement with the fitted EOS results shown in Table II.

C. Electronic band structures

Starting with the atomic geometry given by the optimized crystal structures just discussed, we have calculated the electronic band structures of the pure Sn clathrate frameworks. For comparison, we have also calculated the band structures of α-Sn and β-Sn. We find that α-Sn is a semimetal and that

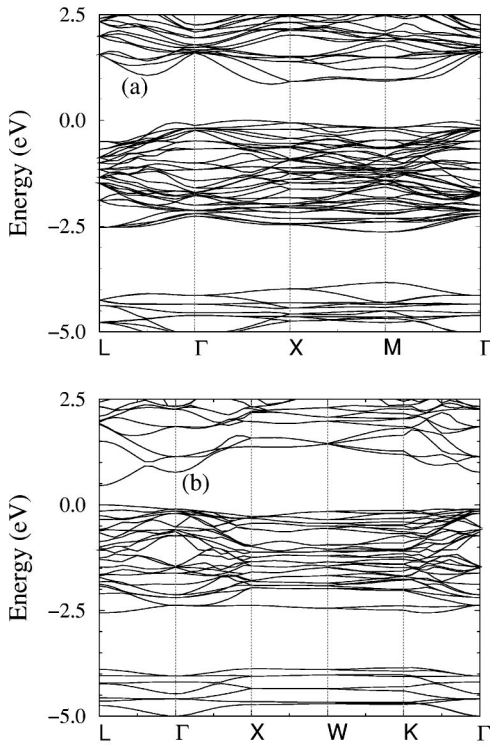

FIG. 2. The near band gap LDA electronic band structures of (a) Sn_{46} and (b) Sn_{136}. In units of $2\pi/a$, the k points correspond to (a) $L=(\frac{1}{2},\frac{1}{2},\frac{1}{2})$, $\Gamma=(0,0,0)$, $X=(\frac{1}{2},0,0)$, and $M=(\frac{1}{2},\frac{1}{2},0)$ and (b) $L=(\frac{1}{2},\frac{1}{2},\frac{1}{2})$, $\Gamma=(0,0,0)$, $X=(1,0,0)$, $W=(1,\frac{1}{2},0)$, and $K=(\frac{3}{2},\frac{3}{2},0)$.

β-Sn is a metal. It is well known that the LDA generally underestimates semiconductor band gaps. In our study of Ge,[16] we found that the LDA underestimates the band gap of diamond-phase Ge by at least 0.7 eV. Following our earlier work on Si and Ge clathrates, we assume that the LDA band gap errors are relatively constant from one structure to the next, so that the predicted trend in the band gap as the structure changes from α-Sn to Sn_{46} to Sn_{136} should be reliable. We note again that we neglect spin-orbit coupling.

Since each Sn atom is tetrahedrally bonded in both clathrate types, one would expect the pristine framework materials Sn_{46} and Sn_{136}, to be semiconductors. Our results are consistent with this. In Figs. 2(a) and 2(b) are shown the calculated band structures of Sn_{46} and Sn_{136}. In these and in subsequent figures, the zero of energy is taken at the top of the valence band. For Sn_{46} [Fig. 2(a)], the flatness of the bands means that the precise k-point to k-point transition where the minimum energy gap occurs cannot accurately be determined. Also small geometric changes in the unit cell structure as well as errors in the LDA are likely to shuffle the band ordering. For this material, we find three distinct valence band maxima which are nearly degenerate. In addition, there are three local conduction band minima. Within this LDA and structural model, we find that Sn_{46} is a semiconductor for which the smallest energy gap is 0.855 eV and for which this minimum gap occurs on the line from the Γ point to the X point. Since the k-point separation is small and the bands (particularly the valence bands), are flat, we feel that it is best to conclude that this material has a ''quasidirect'' band gap. The situation is clearer for Sn_{136}, for which our band structures are shown in Fig. 2(b). We find that this type-II Sn clathrate is a direct band gap semiconductor with a band gap of 0.458 eV which occurs at the L point.

TABLE IV. The cohesive energies and Birch-Murnaghan parameters for the type-I Sn-based clathrate materials obtained from a fit to the LDA energy vs volume curve.

Composition	Cohesive energy (kcal/mol)	V_0 (Å^3/unit cell)	K_0 (GPa)	K'
Sn_{46}	−43	1744.	38.4	4.9
Cs_8Sn_{46}	226	1891.	34.6	3.7
$Cs_8Sn_{44}\square_2$	229	1745.	32.4	5.9
$Cs_8Ga_8Sn_{38}$	290	1705.	42.0	4.9
$Cs_8Zn_4Sn_{42}$	285	1741.	40.4	5.4

IV. BINARY TIN CLATHRATE COMPOUNDS WITH CESIUM GUESTS

A. Energetics, structures, and internal coordinates

We begin our study of the Cs-Sn clathrate compounds with the idealized, fully stoichiometric system Cs_8Sn_{46}, which has the same space group symmetry (O_h) as Sn_{46}. The presence of the large Cs guests expands the Sn framework. Using the same LDA optimization and Birch-Murnaghan procedure as before, we have calculated the EOS of Cs_8Sn_{46}. The results for the parameters V_0, K_0, and K' for Cs_8Sn_{46}, as well as for the other compounds considered in this paper, are shown in Table IV. For ease of comparison, these parameters for pure Sn_{46} are also shown again in this table. In contrast to the previously discussed results of Table II, the parameter V_0 in Table IV is the volume per unit cell, rather than the volume per atom.

As can been seen from Table IV, the expectation of an expanded volume for Cs_8Sn_{46} is realized; we find that the equilibrium volume is larger by about 8.4% in comparison with that of the pristine Sn_{46} framework. The minimum energy parameter E_0 has been omitted from Table IV, since the relative energy has little physical importance when the material compositions are different. Instead, we have used E_0 to estimate the cohesive energy of the Cs-Sn clathrate. To do this, we define the cohesive energy as the energy released in producing one unit cell (one formula unit) of the compound from diamond phase Sn and the elemental metal solid(s). For Cs_8Sn_{46}, this energy can thus be calculated by analyzing the energetics of the reaction

$$46Sn_{\alpha}+8Cs_{A2}\rightarrow Cs_8Sn_{46}. \quad (1)$$

Here, Sn_{α} and Cs_{A2}, respectively, denote α-Sn and Cs in the A_2 phase. A positive cohesive energy in this case favors the formation of Cs-Sn compounds in the clathrate phases. Our calculations find an exothermic reaction which releases 226 kcal/mol (9.826 eV) of energy per Cs_8Sn_{46}. This is a very large energy of formation, particularly when it is noted that the empty Sn clathrate is endothermic compared to the diamond phase. (As shown in Table IV, our calculated cohesive

TABLE V. Experimental structural parameters (cubic lattice constants and fractional internal coordinates) for various Sn-based clathrate materials. These are shown for comparison with the LDA-generated theoretical parameters shown in Table III. The notation for the internal coordinates is the same as in Table III.

		Fractional internal coordinates		
Material	a (Å)	x_i	y_k	z_k
K_8Sn_{46} [a]	12.03	0.1830	0.3100	0.1180
$Rb_8Sn_{44.6}$ [b]	12.054	0.1828	0.3180	0.1189
$K_{1.6}Cs_{6.4}Sn_{44}$ [b]	12.084	0.1829	0.3164	0.1192
$K_8Al_8Sn_{38}$ [c]	12.007	0.1827	0.3158	0.1180
$Rb_8Al_8Sn_{38}$ [c]	12.036	0.1832	0.3137	0.1182
$K_8Ga_8Sn_{38}$ [c]	11.935	0.1831	0.3130	0.1179
$Rb_8Ga_8Sn_{38}$ [c]	11.964	0.1834	0.3120	0.1181
$Ba_8Ga_{16}Sn_{30}$ [c]	11.744	0.18424	0.31229	0.11855
$Cs_8Ga_8Sn_{38}$ [d]	12.0792	0.1832	0.3142	0.1186
$Cs_8Zn_4Sn_{42}$ [d]	12.0928	0.1833	0.3139	0.1190

[a]Reference 22.
[b]Reference 19.
[c]Reference 20.
[d]Reference 21.

energy for pure Sn_{46} is -43 kcal/mol$=-1.8$ eV, which is consistent with the EOS results in Table II and in Fig. 1.) This result (and the other cohesive energies in Table IV) clearly shows that Cs acts as a strong stabilizing agent in the Sn clathrate materials.

Correlating with the framework expansion due to the presence of the larger Cs guests, longer Sn-Sn bonds are expected for Cs_8Sn_{46} than for pristine Sn_{46}. Our results are in agreement with this expectation. The four distinct Sn-Sn bond lengths which we found in Sn_{46} increase in Cs_8Sn_{46} to 2.82, 2.86, 2.89, and 2.93 Å. In comparison with Sn_{46}, we thus predict a 2–4 % bond length expansion. Both the increase in bond lengths and their larger spread indicate a *weakening* in the Sn-Sn bonds. This is consistent with the calculated bulk modulus (Table IV) for Cs_8Sn_{46}, which is about 10% smaller than that for Sn_{46}. The predicted bond angles for this material are very similar to those in Sn_{46}, as they should be since the overall symmetry is preserved. They range from 105.7° to 124.4°. The optimized cubic lattice constant and relative internal coordinates for Cs_8Sn_{46}, along with those of the other considered materials, are given in Table III. Experimental results do not exist for Cs_8Sn_{46}. However, results exist for the lattice constants and internal coordinates for several Sn clathrate materials which are related to this material. These are summarized in Table V for comparison with our theoretical results.

There is experimental evidence that laboratory-synthesized alkali-Sn clathrate compounds contain two vacancies per unit cell at the framework sites.[19,21] X-ray refinement suggests that the vacancies are at the 6*c* sites. The locations of 6*c* sites are at the vertices shared by two hexagons which are perpendicular to each other. Strictly speaking, if the vacancies are randomly distributed over two of the 6*c* sites, these vacancy-containing clathrates are no longer periodic crystals. In the present study, we simplify this problem by making the approximation that the two vacancies per cell are *ordered* within the (large) 46-atom type-I Sn clathrate unit cell. We thus assume that the two vacancies exist at particular (see below) 6*c* sites and we denote the resulting compound by the formula $Cs_8Sn_{44}\square_2$.

All of the 6*c* sites in the type-I clathrate framework are located within the hexagonal rings. One simple way to visualize the spatial distribution of 6*c* sites is by ''isolating'' a 24-atom internal cage. Viewed along the sixfold rotation axis of this cage, one pair of 6*c* sites lies at the opposite ends of the top hexagonal ring, while another pair of 6*c* sites lies on the bottom hexagonal ring, with a 90° rotation with respect to the pair in the top ring. With these unit-cell and ordered-crystal assumptions, there are only two nonequivalent configurations for the two vacancies at the 6*c* sites in $Cs_8Sn_{44}\square_2$. We denote these choices as models I and II. In model I, there are two vacancies located within the same hexagonal ring (i.e., either both on the top or both at the bottom), and the minimal atomic distance is 1/2 of the lattice constant. In model II, the two vacancies are located in different hexagonal rings (i.e., one on top and the other at bottom), and the minimal distance is $\sqrt{6}/4$ (~ 0.6123) of the lattice constant. Using the same optimization and Birch-Murnaghan procedure as before, we have determined the EOS for both models. The results of this procedure then determine the lowest energy model. From these calculations, we find that model II is energetically favored by 0.618 eV/vacancy; quite a large energy. We thus show only the results of model II in Table IV. The much lower energy of model II in comparison with model I is likely caused by the more distant vacancy-vacancy separation. Model II (point group C_{2v}) also has lower symmetry than model I (point group D_{4h}). Because of the entropy term in the free energy, model II should be more energetically favored at finite temperatures.

The optimized lattice constant for model II of $Cs_8Sn_{44}\square_2$ is given in Table III. The internal coordinates of this material are not shown because the placement of the vacancies in this model reduces the cubic symmetry of the Cs_8Sn_{46} structure to tetragonal. See also Table V for comparison of our theoretical prediction with experimental data on compounds

similar to $Cs_8Sn_{44}\square_2$. In addition to the symmetry reduction from cubic to tetragonal, the presence and placement of the vacancies in model II causes considerable distortion in the bond lengths and bond angles from those found in Cs_8Sn_{46}. Instead of the four distinct Sn-Sn bond lengths we have found in the other materials, our calculations find a distribution of bond lengths which range from 2.77 to 2.96 Å. However, the majority of the bond lengths are clustered in the range 2.82 to 2.87 Å, with the ones outside this 0.05 Å, range belonging to bonds which are very near to one of the vacancies. Similarly, our predicted bond angles are also distributed over a very wide range from 96.6° to 123.6°, with the majority clustered in the range 104.2° to 116.2°. The bond angles outside this range belong to bonds which are very near to one of the vacancies.

B. Vacancy formation in the Cs-Sn clathrates

An understanding of vacancy formation in the type-I Sn clathrates can be obtained from further analysis of the relative energetics of Cs_8Sn_{46} and $Cs_8Sn_{44}\square_2$. As just discussed, the LDA shows a weakening of the Sn-Sn bonds in Cs_8Sn_{46}. Further, our electronic band structure calculations (discussed below) show that this material can be viewed as a highly doped tetrahedral semiconductor which is (semi)metallic. Our electronic structure calculations further show that $Cs_8Sn_{44}\square_2$ is a semiconductor in which the donated Cs electrons fill midgap states induced by the Sn vacancies. As a result of this, $Cs_8Sn_{44}\square_2$ is found to have a greatly reduced band gap in comparison with pristine Sn_{46}. The vacancy formation energy which transforms Cs_8Sn_{46} into $Cs_8Sn_{44}\square_2$ can be interpreted as a competition between the energy gained from the Cs-guest donated conduction electrons dropping into the midgap electron states and the energy cost of breaking an Sn-Sn bond to remove a Sn atom.

The total energy of vacancy formation (E_V) in Cs_8Sn_{46} which results in that material transforming to the vacancy compound $Cs_8Sn_{44}\square_2$ plus excess Sn, can be computed directly in density functional theory. This energy is determined from the energetics of the reaction

$$Cs_8Sn_{46} \leftrightarrow Cs_8Sn_{44}\square_2 + 2Sn_\alpha . \tag{2}$$

An analysis of the energetics of this reaction gives

$$2E_V = (44+8)E^0(Cs_8Sn_{44}\square_2) + 2E^0(Sn_\alpha) - (46+8)E^0(Cs_8Sn_{46}). \tag{3}$$

Here $E^0(Cs_8Sn_{44}\square_2)$, $E^0(Cs_8Sn_{46})$, and $E^0(Sn_\alpha)$ are, respectively, the binding energies per atom for $Cs_8Sn_{44}\square_2$, Cs_8Sn_{46}, and α-Sn.

We have computed each energy on the right side of Eq. (3) within the LDA. This yields a vacancy formation energy of $E_V = -0.065$ eV/vacancy. The negative value indicates that vacancy formation in these materials is favorable (at $T = 0$ K), which is in agreement with experiment. This vacancy formation energy is consistent with the cohesive energy we have computed for $Cs_8Sn_{44}\square_2$, which is 229 kcal/mole (Table IV). This estimate of the vacancy formation energy is based on model II. A similar estimation based on model I gives a value of $E_V = +0.553$ eV/vacancy, which suggests that vacancy formation is not favored for this configuration. Based on these results, we conclude that $Cs_8Sn_{44}\square_2$ is stable, and that Cs_8Sn_{46} will tend to transform to $Cs_8Sn_{44}\square_2$. This result also suggests that vacancies on the $6c$ sites are unlikely to be randomly distributed. Further, the results for model I indicate that a configuration with two vacancies within the same hexagonal ring is not energetically favored.

C. Electronic band structures

Starting with the optimized atomic geometry for the two binary Cs-Sn materials just discussed, we have calculated the electronic band structures for $Cs_8Sn_{44}\square_2$ and Cs_8Sn_{46}. Qualitatively, one expects that the eight unsaturated bonds left by the two vacancies in $Cs_8Sn_{44}\square_2$ will become lone pairs as the eight valence electrons donated by the Cs guests fill them up. Hence, this compound is expected to be a semiconductor. By contrast, Cs_8Sn_{46} is expected to be metallic, since all framework bonds in that material are satisfied by the electrons from the Sn host, forcing the eight Cs electrons to occupy the lowest-lying antibonding states (conduction bands) of the Sn framework. This qualitative discussion implicitly assumes a ''rigid band'' approximation for the Sn framework-derived bands, ignores any band shifting or rehybridization produced by the Cs, and ignores the lowered symmetry of $Cs_8Sn_{44}\square_2$ in comparison with Sn_{46} and Cs_8Sn_{46}. The calculated band structures for Cs_8Sn_{46} and $Cs_8Sn_{44}\square_2$ are shown in Figs. 3(a) and 3(b), respectively. The qualitative ''rigid band'' picture just described is confirmed by these LDA results.

In order to best understand the metallic band structure of Cs_8Sn_{46} [Fig. 3(a)], and in order to enable an easy quantitative comparison with the bands of the other materials, we choose the zero of energy to lie at the top of the Sn_{46}-derived valence band. The ''pseudo-band-gap'' between these bands and the bottom of the lowest-lying conduction band is 0.526 eV. This occurs between k points that both lie along the Γ to X line. Donor electrons from Cs occupy these higher energy states, and the Fermi-level lies in the conduction bands at 1.13 eV. Comparison of the shapes of various bands for Cs_8Sn_{46} with those of the Sn_{46} framework [Fig. 2(a)] shows that the ''rigid-band'' picture discussed above is qualitatively correct. This picture asserts that the bands for the guest-containing material are nearly the same as those of the framework and that the system simply raises its Fermi level to accommodate the guest electrons. Another effect of the Cs electrons on the Sn_{46} band structure is to lower the conduction bands towards the valence bands, decreasing the pseudo-band-gap. As may be seen in Fig. 3(a), we find three distinct valence band maxima, which are nearly degenerate and three local conduction band minima.

There is a large qualitative change in the bands of the compound $Cs_8Sn_{44}\square_2$ [Fig. 3(b)] compared with those for Cs_8Sn_{46}. As is shown in Fig. 3(b), we find that $Cs_8Sn_{44}\square_2$ is a very narrow gap semiconductor. As already mentioned, the lattice symmetry in this material is reduced from the cubic symmetry of Cs_8Sn_{46} to tetragonal. Hence, in Fig. 3(b) we

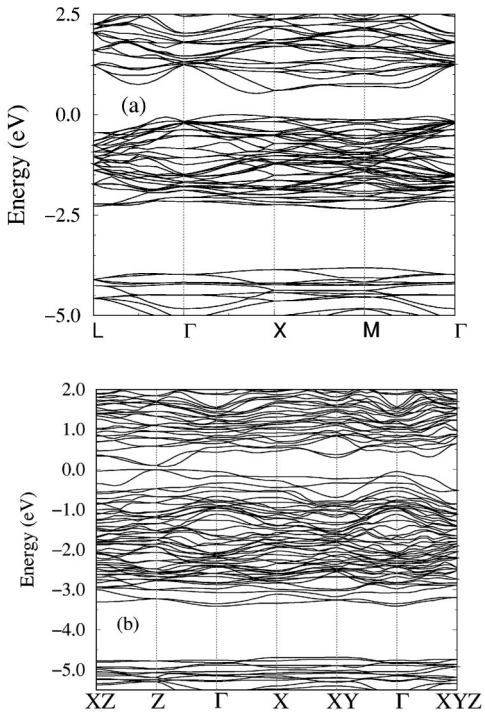

FIG. 3. The near band gap LDA electronic band structures of (a) cubic type I Cs_8Sn_{46} and (b) tetragonal $Cs_8Sn_{44}\square_2$. In (a), the Fermi level is at 1.13 eV. The tetragonal model II for $Cs_8Sn_{44}\square_2$ has been assumed. In units of $2\pi/a$ and $2\pi/c$, the k points in the tetragonal (b) unit cell correspond to $XZ=(\frac{1}{2},0,\frac{1}{2})$, $Z=(0,0,\frac{1}{2})$ $\Gamma=(0,0,0)$, $X=(\frac{1}{2},0,0)$, $XY=(\frac{1}{2},\frac{1}{2},0)$, and $XYZ=\frac{1}{2},\frac{1}{2},\frac{1}{2})$. See the caption of Fig. 2(a) for the k points of the cubic cell.

have plotted the bands along the line from the Γ point to the Z point in the Brillouin zone, as well as from the Γ point to the X point. As can be seen in the figure, both the shape of the bands and the resulting band gap are qualitatively quite different along these two directions. We find that the minimum band gap is approximately 0.07 eV and that it occurs along the Γ to Z line, near the Z point. In this regard, we point out again that the LDA is known to underestimate band gaps. In this material, we also find three distinct, nearly degenerate, valence band maxima and three local conduction band minima.

Despite the lowering of the symmetry, the ''rigid-band'' picture is still useful to obtain a qualitative understanding of the bands for this material. In particular, several vacancy-derived states (''dangling-bond'' levels) can be identified. These lie within the Sn_{46} derived band gap [compare with Fig. 2(a)]. These levels are fully occupied, and reduce the band gap to the mentioned value. The vacancies and the resulting lattice distortion have clearly drastically altered both the shapes of the valence and conduction bands and their positions in comparison with the bands of Cs_8Sn_{46}.

V. TERNARY TIN CLATHRATE COMPOUNDS

A. Energetics, structures, and internal coordinates

A class of more complex clathrate compounds is that with both donor alkali guest atoms inside the cages and substitutional acceptor atoms replacing some of the framework atoms. A clathrate framework which contains both group IV (B) (host) atoms and acceptor (impurity) atoms can be viewed as an alloy. Compounds based on type I clathrates have been synthesized both with single acceptor (group III) atoms and with double acceptor (group II) atoms replacing some of the group IV (B) atoms. As prototype materials for the present study, we choose two such Sn clathrate-based materials: $Cs_8Ga_8Sn_{38}$, in which the Ga atoms act as single acceptors, and $Cs_8Zn_4Sn_{42}$, in which the Zn atoms act as double acceptors. Both of these materials have recently been synthesized and have been suggested for possible thermoelectric applications.[21]

Introducing electron acceptors, such as Ga or Zn, into the clathrate framework is expected to stabilize the lattice and to prevent vacancy formation. Since the acceptor atoms are charged, their location in the lattice has important effects on the energetics of these materials. In order to avoid the difficult task of treating random Sn/Ga or Sn/Zn clathrate alloys, we have constructed symmetric, ordered structural models for these compounds. Following the guidelines we have previously found and used successfully for alloyed Ge clathrates,[17] we have assumed that there are no nearest-neighbor Ga-Ga or Zn-Zn bonds in the lattice structure. In addition, for $Cs_8Ga_8Sn_{38}$, we have assumed that the eight Ga atoms occupy half of the 16i sites. There is one unique symmetry way to accomplish this, which reduces the point group symmetry from O_h to T_d. For $Cs_8Zn_4Sn_{42}$, we have used the results of recent x-ray data[21] and have assumed that the substitutional Zn atoms are on 6c sites. Similar to $Cs_8Sn_{44}\square_2$, there are two ways to construct such a model of $Cs_8Zn_4Sn_{42}$. Here, we concentrate on the model with C_{2v} symmetry. This is similar to model II for $Cs_8Sn_{44}\square_2$.

Using the same optimization and Birch-Murnaghan procedure as before, and using the assumptions just discussed for the lattice structures of $Cs_8Ga_8Sn_{38}$ and $Cs_8Zn_4Sn_{42}$, we have calculated their EOS's. The parameters of a fit to a Birch-Murnaghan EOS for $Cs_8Ga_8Sn_{38}$ and $Cs_8Zn_4Sn_{42}$ are shown in Table IV. As may be seen in that table, the equilibrium volume V_0 of $Cs_8Ga_8Sn_{38}$ is about 98% of that of the pure Sn_{46} framework, while, that for $Cs_8Zn_4Sn_{42}$ is almost identical to that of Sn_{46}. Further, the predicted equilibrium bulk modulus K_0 for $Cs_8Ga_8Sn_{38}$ is about 9.4% larger than that for Sn_{46}, while that for $Cs_8Zn_4Sn_{42}$ it is about 4.9% larger. As before, instead of directly showing the minimum energy parameter E_0 in Table IV, we have used our results for these to estimate the cohesive energies of these materials. The predicted cohesive energies for $Cs_8Ga_8Sn_{38}$ and $Cs_8Zn_4Sn_{42}$ are 290 and 285 kcal/mole, respectively.

We have also optimized the internal atomic coordinates for these materials. We first discuss $Cs_8Ga_8Sn_{38}$. The framework of this material expands due to the Cs in the cages, and there is also considerable framework distortion due to the presence of the smaller Ga atoms on some of the Sn sites. We find three distinct Sn-Sn bond lengths (2.83, 2.84, and 2.89 Å). The Sn-Sn bond length is thus expanded by 2 to 4 % over those in Sn_{46}. Based on atomic radii, the Ga-Sn bond lengths are expected to be shorter than the Sn-Sn bond length. Our results confirm this. Two distinct Ga-Sn bond lengths are

found, 2.61, and 2.65 Å. We find three distinct types of framework bond angles. The (Sn-Ga-Sn) bond angles range from 108.75° to 110.2°, the (Ga-Sn-Sn) bond angles range from 108.1° to 112.3°, and the (Sn-Sn-Sn) bond angles range from 101.0° to 113.9°. For the assumed arrangement of Ga atoms in the framework, there are no (Ga-Sn-Ga) bond angles. The optimized lattice constant is shown in Table III. Again, the internal coordinates of this material are not shown because it does not have the symmetry of Sn_{46} and Cs_8Sn_{46}. See also Table V for comparison of our theoretical prediction with experimental data on $Cs_8Ga_8Sn_{38}$ and similar compounds.

For $Cs_8Zn_4Sn_{42}$, we again find considerable framework expansion and distortion due to Cs in the cages and to the presence of the smaller Zn atoms on four of the Sn sites. There are several distinct Sn-Sn bond lengths, which range from 2.78 to 2.90 Å. This is similar to the range found for Cs_8Sn_{46} and results in a similar large bond length spread. However, the majority of the Sn-Sn bond lengths are in the range 2.79 to 2.84 Å. The Sn-Zn bonds are considerably shorter than the Sn-Sn bonds, as is expected from atomic radii considerations. There are two distinct Zn-Sn bond lengths of 2.62 and 2.65 Å, and there are three types of bond angles. The (Sn-Zn-Sn) bond angles range from 107.9° to 110.8°, the (Zn-Sn-Sn) bond angles range from 108.3° to 128.0°, and the (Sn-Sn-Sn) bond angles range from 99.9° to 122.2°. For our model structure, no (Zn-Sn-Zn) bond angles exist.

Table III shows the optimized lattice constant for $Cs_8Zn_4Sn_{42}$. See also Table V, which contains experimental data on $Cs_8Zn_4Sn_{42}$ and similar compounds for comparison with our theoretical predictions. The internal coordinates of this material are not shown because it does not have the same symmetry as Sn_{46} and Cs_8Sn_{46}.

B. Electronic band structures

We have performed electronic band-structure calculations for the two Sn clathrate compounds $Cs_8Ga_8Sn_{38}$ and $Cs_8Zn_8Sn_{42}$. The atomic geometries used in these calculations are the optimized structures just discussed. Since the LDA generally underestimates semiconductor band gaps, we again assume that the band gap errors are relatively constant from one structure to the next. Thus, the trends in the band gap as the material composition is changed from Sn_{46} should be meaningful.

In $Cs_8Ga_8Sn_{38}$, the substitutional Ga acceptors are compensated by interstitial Cs donors and this compound should be a semiconductor. Similarly, one expects $Cs_8Zn_8Sn_{42}$ also to be semiconducting if Zn acts as a double acceptor. These simple conclusions again assume a ''rigid band'' approximation for the Sn framework-derived bands, and they ignore the band shifting and hybridization effects caused by the donors and acceptors. That such a picture holds is not obvious since the ''doping'' levels of these materials is enormous[23] when measured by the standards of conventional electronic materials. However, this qualitative picture is indeed confirmed by our detailed calculations.

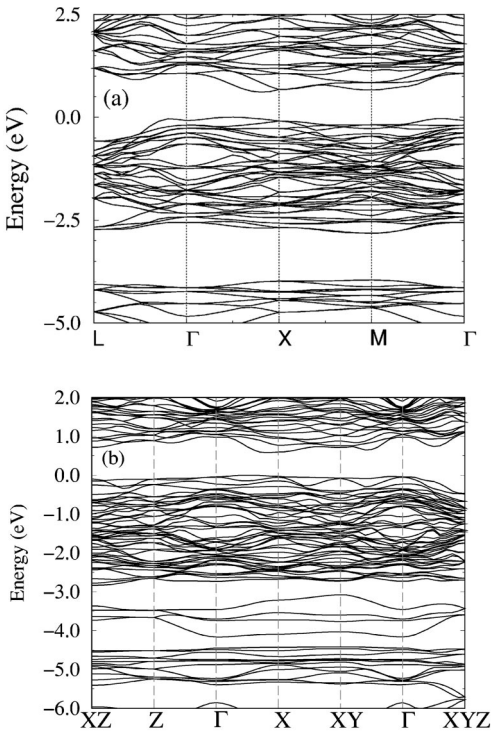

FIG. 4. The near band gap LDA electronic band structures of (a) $Cs_8Ga_8Sn_{38}$ (T_d symmetry) and (b) $Cs_8Zn_4Sn_{42}$ (C_{2v} symmetry). The ordered ''alloy'' models assumed for these materials are discussed in the text.

In Figs. 4(a) and 4(b), we show the band structures for $Cs_8Ga_8Sn_{38}$ and $Cs_8Zn_4Sn_{42}$, respectively. The zero of energy is taken at the top of the valence band. As mentioned above, our model of $Cs_8Zn_4Sn_{42}$ has tetragonal symmetry. Hence, in Fig. 4(b) we have plotted the bands along the Γ to Z line, as well as from Γ to X. In agreement with the qualitative, ''rigid band'' picture just discussed, we find that $Cs_8Ga_8Sn_{38}$ and $Cs_8Zn_4Sn_{42}$ are semiconductors with band gaps of 0.619 and 0.574 eV, respectively. Comparison of the shapes of various bands for the compounds is also consistent with this qualitative picture. For example, comparison of the bands for $Cs_8Ga_8Sn_{38}$ [Fig. 4(a)] with those of Cs_8Sn_{46} [Fig. 3(a)] shows that the alloying of Ga in the Sn framework changes little the overall shape of the upper valence and lower conduction bands. Similar statements can be made about the bands of $Cs_8Zn_4Sn_{42}$ [Fig. 4(b)].

For reasons similar to those discussed above for the other materials, the precise k-point to k-point transition for the minimum energy gap is probably not meaningful. For both $Cs_8Ga_8Sn_{38}$ and $Cs_8Zn_4Sn_{42}$ [Figs. 4(a) and 4(b)], we find three distinct valence band maxima which are nearly degenerate as well as three local minima in the conduction bands. Within the LDA and the structural models for these materials, the smallest energy gap in both cases is direct; between bands at k points that lie along the Γ to X line.

VI. SUMMARY

Using the LDA, we have determined the equilibrium structural parameters, the equations of state, and the elec-

tronic band structures of the following Sn-based clathrate materials: Sn_{46}, Sn_{136}, Cs_8Sn_{46}, $Cs_8Sn_{44}\square_2$, $Cs_8Ga_8Sn_{38}$, and $Cs_8Zn_4Sn_{42}$. The minimum binding energies we find for the pure Sn clathrates are $\sim$38 meV/atom (Sn_{136}) and $\sim$41 meV/atom (Sn_{46}) higher that that of α-Sn, and their volumes per atom are larger than that of α-Sn by $\sim$12% (Sn_{46}) and $\sim$14% (Sn_{136}). We find that all materials considered are semiconductors except for Cs_8Sn_{46}, which is metallic. For the semiconductors, we find band gaps of 0.855 eV (Sn_{46}), 0.610 eV ($Cs_8Ga_8Sn_{38}$), 0.574 eV ($Cs_8Zn_4Sn_{42}$), 0.07 eV ($Cs_8Sn_{44}\square_2$), and 0.458 eV (Sn_{136}).

In order to obtain an understanding of vacancy formation in the type-I Sn clathrates with Cs guests, we have also computed the energy of vacancy formation E_V in the reaction which transforms Cs_8Sn_{46} to $Cs_8Sn_{44}\square_2$ plus excess Sn. Within an ordered model of $Cs_8Sn_{44}\square_2$, we find $E_V = -0.065$ eV/vacancy. Thus, in qualitative agreement with experiment, we find that vacancy formation is favored in this system (at $T=0$).

Clathrate materials based on Sn are currently being studied experimentally for thermoelectric and electronic materials applications. We hope that our predictions will prove useful in better understanding such experiments.

ACKNOWLEDGMENTS

We thank the NSF for Grants No. DMR-99-86706 and No. DMR-96-32635, through ASU MRSEC which partially supported this work. We thank Dr. Ganesh K. Ramachandran, Professor Paul F. McMillan (Arizona State University/ University College London/Royal Institution Great Britain), Professor Jan Gryko (Jacksonville State University), and Professor George Nolas (University of South Florida) for many helpful discussions. C.W.M. thanks Texas Tech University for a Faculty Development Leave which enabled him to carry out this work and the Department of Physics and Astronomy at Arizona State University for their hospitality while a portion of this work was done. J.D. acknowledges the support from his Auburn University start-up fund and many insightful discussions with Professor A.-B. Chen (Auburn University).

[1] D. A. Young, *Phase Diagrams of the Elements* (University of California Press, Oxford, England, 1991), pp. 106–107.

[2] I. N. Nikolaev, V. P. Mar'in, V. N. Panyushkin, and L. S. Pavlyukov, Sov. Phys. Solid State **14**, 2022 (1973).

[3] W. F. Claussen, J. Chem. Phys. **19**, 259 (1951); **19**, 1425 (1951); L. Pauling and R. E. Marsh, Proc. Natl. Acad. Sci. U.S.A. **36**, 112 (1952).

[4] J. S. Kasper, P. Hagenmuller, M. Pouchard, and C. Cros, Science **150**, 1713 (1965).

[5] C. Cros, M. Pouchard, and P. Hagenmuller, C. R. Seances Acad. Sci. Ser. A **260**, 4764 (1965).

[6] C. Cros, M. Pouchard, P. Hagenmuller, and J. S. Kasper, Bull. Soc. Chim. Fr. **7**, 2737 (1968).

[7] C. Cros, M. Pouchard, and P. Hagenmuller, J. Solid State Chem. **2**, 570 (1970); Bull. Soc. Chim. Fr. **2**, 379 (1971).

[8] J. Gryko, P. F. McMillan, R. F. Marzke, A. P. Dodokin, A. A. Demkov, and O. F. Sankey, Phys. Rev. B **57**, 1 (1998); G. K. Ramachandran, J. J. Dong, J. Diefenbacher, J. Gryko, O. F. Sankey, R. F. Marzke, M. O'Keeffe, and P. F. McMillan, J. Solid State Chem. **145**, 716 (1999).

[9] S. Bobev and S. C. Sevov, J. Am. Chem. Soc. **121**, 3795 (1999).

[10] G. B. Adams, M. O'Keeffe, A. A. Demkov, O. F. Sankey, and Y. Huang, Phys. Rev. B **49**, 8048 (1994).

[11] A. A. Demkov, O. F. Sankey, K. E. Schmidt, G. B. Adams, and M. O'Keeffe, Phys. Rev. B **50**, 17 001 (1994).

[12] S. Saito and A. Oshiyama, Phys. Rev. B **51**, R2628 (1995).

[13] V. I. Smelyansky and J. S. Tse, Chem. Phys. Lett. **264**, 459 (1997).

[14] J. Dong, O. F. Sankey, and G. Kern, Phys. Rev. B **60**, 950 (1999).

[15] P. Melinon, P. Keǵhelian, X. Blase, J. LeBruse, A. Perez, E. Reny, C. Cros, and M. Pouchard, Phys. Rev. B **58**, 1 (1998); A. San-Miguel, P. Kéghélian, X. Blase, P. Mélinon, A. Perez, J. P. Itié, A. Polian, E. Reny, C. Cros, and M. Pouchard, Phys. Rev. Lett. **83**, 5290 (1999).

[16] J. Dong and O. F. Sankey, J. Phys.: Condens. Matter **11**, 6129 (1999).

[17] J. Dong, O. F. Sankey, G. K. Ramachandran, and P. F. McMillan, J. Appl. Phys. **87**, 7726 (2000).

[18] N. P. Blake, L. Mollnitz, G. Kresse, and H. Metiu, J. Chem. Phys. **1111**, 3133 (1999); J. Zhao, A. Buldum, J. P. Lu, and C. Y. Fong, Phys. Rev. B **60**, 14 507 (1999).

[19] J.-T. Zhao and J. D. Corbett, Inorg. Chem. **33**, 5721 (1994).

[20] R. Kroner, K. Peters, H. G. von Schnering, and R. Nesper, Z. Kristallogr.-New Cryst. Struct. **213**, 664 (1998); **213**, 667 (1998); **213**, 669 (1998); **213**, 671 (1998); **213**, 675 (1998); **213**, 677 (1998); **213**, 679 (1998); H. G. Von Schnering, R. Kroner, M. Baitinger, K. Peters, R. Nesper, and Y. Grin, Z. Kristallogr.-New Cryst. Struct. **215**, 205 (2000); S. Bobev and S. Sevov, Mater. Res. Soc Symp. Proc. **626**, Z13.5.1 (2000).

[21] G. S. Nolas, B. C. Chakoumakos, B. Mahieu, G. L. Long, and T. J. R. Weakley, Chem. Mater. **12**, 1947 (2000); G. S. Nolas, T. R. J. Weakley, and J. L. Cohn, *ibid.* **11**, 2470 (1999); G. S. Nolas, in *Thermoelectric Materials 1998*, edited by T. M. Tritt *et al.*, MRS Symposia Proceedings No. 545 (Materials Research Society, Pittsburgh, 1999), pp. 435–442; G. S. Nolas and C. A. Kendziora, Phys. Rev. B **62**, 7157 (2000).

[22] J. Gallmeier, H. Schafer, and A. Weiss, Z. Naturforsch. B **24**, 665 (1969); W. Westerhaus and H.-U. Schuster, *ibid.* **32**, 1365 (1977).

[23] An estimate of the donor "doping" density present in type-I clathrates which are fully loaded with (single donor) alkali guests in the cages can be made by taking Cs_8Sn_{46} as an example. Assume that each Cs atom donates one electron to the conduction band of the Sn_{46} host framework. The minimum volume V_0 we find for Cs_8Sn_{46} is 1891 $Å^3$/unit cell (see Table IV). The concentration of donor electrons from the Cs guests is thus (8/1891) $Å^{-3} = 4.2\times10^{21}$ cm^{-3}, which is three or more orders of magnitude larger than the typical doping concentration in heavily doped Si.

[24] G. K. Ramachandran, P. F. McMillan, J. Diefenbacher, J. Gryko, J. Dong, and O. F. Sankey, Phys. Rev. B **60**, 12 294 (1999).
[25] G. K. Ramachandran, P. F. McMillan, J. Dong, and O. F. Sankey, J. Solid State Chem. **154**, 626 (2000).
[26] S. Bobev and S. C. Sevov, J. Solid State Chem. **153**, 92 (2000).
[27] G. Mahan, B. Sales, and J. Sharp, Phys. Today **50**, 42 (1997).
[28] F. J. Di Salvo, Science **285**, 703 (2000).
[29] G. A. Slack *Thermoelectric Materials - New Directions and Approaches*, edited by T. M. Tritt, G. Mahan, H. B. Lyon, Jr., and M. G. Kanatzidis (Materials Research Society, Pittsburg, PA, 1997), Vol. 478, p. 47.
[30] G. A. Slack, in *CRC Handbook of Thermoelectrics*, edited by D. M. Rowe (CRC, Boca Raton, FL, 1995), p. 407.
[31] G. S. Nolas and G. A. Slack, Am. Sci. **89**, 136 (2001).
[32] T. M. Tritt, Science **283**, 804 (1999).
[33] L. Mihaly, Nature (London) **395**, 839 (1998); V. Keppens *et al.*, *ibid.* **395** 876 (1998).
[34] G. S. Nolas, D. T. Morelli, and T. M. Tritt, Annu. Rev. Mater. Sci. **29**, 89 (1999).
[35] G. S. Nolas, J. L. Cohen, G. A. Slack and S. B. Schujman, Appl. Phys. Lett. **73**, 178 (1998).
[36] G. S. Nolas, T. R. J. Weakley, J. L. Cohn, and R. Sharma, Phys. Rev. B **61**, 3845 (2000).
[37] J. Dong, O. F. Sankey, and C. W. Myles, Phys. Rev. Lett. **86**, 2361 (2001).
[38] C. W. Myles, J. Dong, O. F. Sankey, C. A. Kendziora, and G. S. Nolas (unpublished).
[39] The calculations have been performed using the Vienna Ab initio Simulation Program (VASP), developed at the Institut für Theoretische Physik of the Technische Universität Wien. G. Kresse and J. Furthmüller, Comput. Mater. Sci. **6**, 15 (1996).
[40] G. Kresse and J. Hafner, Phys. Rev. B **47**, 558 (1993); G. Kresse and J. J. Furthmüller, *ibid.* **54**, 11169 (1996).
[41] D. M. Ceperley and B. J. Alder, Phys. Rev. Lett. **45**, 566 (1980).
[42] Y. Guyot, B. Champagnon, E. Reny, C. Cros, M. Pouchard, P. Melinon, A. Perez, and I. Gregora, Phys. Rev. B **57**, R9475 (1997).
[43] D. Vanderbilt, Phys. Rev. B **41**, 7892 (1990); K. Laasonen, R. Car, C. Lee, and D. Vanderbilt, *ibid.* **43**, 6796 (1991).
[44] G. Kresse and J. Hafner, J. Phys.: Condens. Matter **6**, 8245 (1994); G. Kresse and J. Hafner, Phys. Rev. B **48**, 13 115 (1993).
[45] B. H. Cheong and K. J. Chang, Phys. Rev. B **44**, 403 (1991).
[46] N. E. Christensen and M. Methfessel, Phys. Rev. B **48**, 5797 (1993).
[47] P. Pavone, S. Baroni, and S. Gironcoli, Phys. Rev. B **57**, 10 421 (1998); R. Ravelo and M. Baskes, Phys. Rev. Lett. **79**, 2482 (1997).
[48] F. Birch, J. Geophys. Res. **57**, 227 (1952).
[49] The Birch-Murnaghan equation for the energy E as a function of volume V is $E(V)=E_0+\frac{9}{8}KV_0[(V_0/V)^{2/3}-1]^2\{1+[(4-K')/2][1-(V_0/V)^{2/3}]\}$.